CDF/ANAL/JET/PUBLIC/8556

Version 1.4

February 23, 2007

Particle Momentum Correlations in Jets.

S.Jindariani, A.Korytov

University of Florida

A.Pronko

Fermilab

on behalf of the CDF collaboration.

Abstract

We present the first measurement of two-particle momentum correlations in jets produced in $p\bar{p}$ collisions at center of mass energy of 1.96 TeV. Results are obtained for charged particles within a restricted cone with an opening angle of 0.5 radians around the jet axis and for dijet events with masses ranging from 70 to 560 GeV/c^2. Comparison of the experimental data to the theoretical predictions obtained for partons within the framework of resummed perturbative QCD (Next-to-Leading Log Approximation) shows that the parton momentum correlations survive the hadronization stage of jet fragmentation, thus giving further support to the hypothesis of Local Parton-Hadron Duality. The extracted value of NLLA parton shower cut-off scale Q_{eff} was found to be 139 ± 85 MeV.

I. INTRODUCTION

The goal of this analysis is to measure two-particle momentum correlation in jets, study its evolution with jet energy and compare the results to analytical Next-to-Leading-Log Approximation (NLLA) predictions.

The evolution of jets is driven by the emission of gluons at very small transverse momentum with respect to the jet axis. Analytical predictions are based on NLLA [1] calculations supplemented with the hypothesis of Local Parton-Hadron Duality (LPHD) [2]. NLLA provides an analytical description of parton shower formation, while LPHD states that the hadronization process takes place locally, and, therefore, properties of hadrons and partons at the end of the parton shower are closely related. Detailed studies of jet fragmentation allow one to better understand the relative roles of perturbative parton showering and non-perturbative hadronization in shaping the main jet characteristics. Past experimental studies of inclusive distributions of particles in jets [3][4][5] have shown good agreement with theoretical predictions, suggesting that the perturbative QCD (pQCD) stage of jet formation must be dominant, and the role of the non-perturbative stage is reduced to converting final partons into hadrons without significantly affecting the multiplicities and momenta. This paper addresses the question of whether more subtle effects, such as momentum correlation, also survive hadronization. The predictions for the parton momentum correlations at the level of NLLA precision were first obtained in [6] and recently updated in [7].

Until now, the two-particle momentum correlations were studied only by the OPAL collaboration [8]. The measurement was made in e^+e^- collisions at center of mass energy ~ 91 GeV and exclusively for quark jets in the final state. All particles in the full experimentally accessible stereo-angle were used in the analysis. This allowed to avoid the question of jet reconstruction, but clearly went beyond the range where the theory was valid. Strictly speaking, the theory controls parton shower development only within a small opening angle θ_c around the jet axis, so that $\tan\theta_c \sim \theta_c$. The measured distributions showed the pattern qualitatively agreeing with the predictions, but the fitted values of Q_{eff} were by far inconsistent with Q_{eff} extracted from the fits of the inclusive momentum distributions [9].

Compared to measurement at an e^+e^- collider, a measurement of the two-particle momentum correlation at a $p\bar{p}$ collider takes advantage of a wide range of jet energies, allowing one to explore the evolution of correlation parameters with energy.

In this paper, we report a measurement of the two-particle momentum correlation for charged particles in events with dijet invariant masses in the range 70-560 GeV/c^2. Events were produced at the Tevatron collider in $p\bar{p}$ collisions at a center of mass energy of 1.96 TeV and were recorded by the CDF Run II detector. The total integrated luminosity was 385 pb^{-1}.

The data sample consists of two-jet events with a mixture of quark and gluon jets in the final state. In order to compare experimental results with theoretical predictions, the analysis is carried out in the center-of-mass system of the two jets. The data are divided into seven dijet invariant mass bins. Momentum correlation distributions are measured for charged particles in restricted cones with small opening angle of $\theta_c = 0.5$ radians around jet axis.

The measured distributions are fit to NLLA analytical functions with three free parameters, c_0, c_1 and c_2. These parameters define the strength of the correlation. The fits of their evolution with jet hardness are used to extract the value of the parton shower cutoff Q_{eff}. Fits are done separately for each of the three parameters c_0, c_1 and c_2.

The correlations observed in data are also compared to Monte Carlo predictions by Pythia Tune A [10][11] and Herwig 6.5 [12] event generators.

II. THEORETICAL CONSIDERATIONS

A. Next-to-Leading Log Approximation

NLLA allows one to perform a resummed perturbative calculation of the parton shower by keeping terms $\alpha_s^n \log^{2n}(E_{jet})$ and $\alpha_s^n \log^{2n-1}(E_{jet})$ (where E_{jet} is the energy of a jet and α_s is strong coupling constant) at all orders n of perturbation theory. To describe jet fragmentation successfully, a theoretical model must be able to handle particle emissions at very low transverse momentum k_t with respect to the jet axis. However, most of the particles in jets have k_T well below 1 GeV/c and, therefore, are in the region where traditional perturbative QCD calculations fail.

In NLLA, a sufficiently high cut-off scale Q_{cutoff} is selected to ensure that for all partons with $k_T > Q_{cutoff}$ the perturbative calculations can be applied. After the resummation, the value of the parameter Q_{cutoff} can often be lowered to the value of Λ_{QCD}. This is equivalent

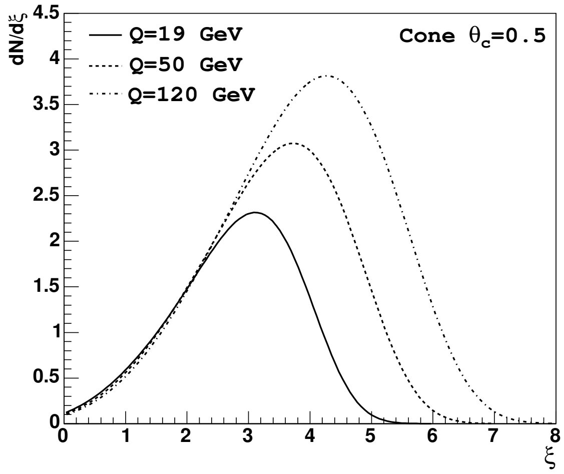

FIG. 1: NLLA inclusive momentum distributions for $Q = 19, 50$ and 120 GeV and $Q_{eff} = 230$ MeV.

to including softer partons in the description of the model and maximizing the range of its applicability. The phenomenological scale replacing the two initial parameters Q_{cutoff} and Λ_{QCD} is conventionally called Q_{eff}.

The inclusive momentum distribution function of particles in jets $D(\xi) = \frac{dN}{d\xi}$ in NLLA is defined in terms of the variable $\xi = \log(\frac{1}{x})$ where $x = \frac{p}{E_{jet}}$ and p is the parton momentum. It is predicted to have a distorted gaussian shape [13]. The position of its maximum depends on the so-called jet hardness $Q = E_{jet}\theta_c$. The evolution of the NLLA predicted inclusive momentum distribution with jet hardness is shown in Fig. 1 [6].

In NLLA, the two-particle momentum correlation function $R(\Delta\xi_1, \Delta\xi_2)$ is defined as a ratio of two- and one- particle momentum distribution functions:

$$R(\Delta\xi_1, \Delta\xi_2) = \frac{D(\xi_1, \xi_2)}{D(\xi_1)D(\xi_2)}, \tag{1}$$

where $D(\xi_1, \xi_2) = \frac{d^2N}{d\xi_1 d\xi_2}$, $\Delta\xi = \xi - \xi_0$ and ξ_0 is the position of the maximum of $D(\xi)$. The momentum distributions are normalized as follows: $\int D(\xi)d\xi =< n >$, where $< n >$ is the average multiplicity of partons in a jet, and $\int\int D(\xi_1, \xi_2)d\xi_1 d\xi_2 =< n(n-1) >$ for all pairs of different partons in a jet. Average multiplicity of particles $< n >$ is a function of the dijet mass M_{jj} and the size of an opening angle θ_c. For $\theta_c = 0.47$ it varies from 5.98 ± 0.63 for $M_{jj} = 82$ GeV/c^2 to 11.97 ± 1.30 for $M_{jj} = 628$ GeV/c^2 [4].

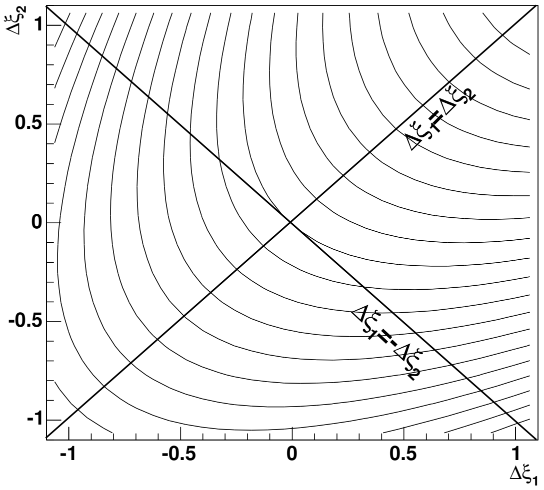

FIG. 2: Shape of the NLLA correlation distribution function.

The NLLA approximation of Eq. (1) for the two-particle momentum correlation function in a jet is

$$R(\Delta\xi_1, \Delta\xi_2) = r_0 + r_1(\Delta\xi_1 + \Delta\xi_2) + r_2(\Delta\xi_1 - \Delta\xi_2)^2, \tag{2}$$

where parameters r_0, r_1 and r_2 define the strength of the correlation and depend on the variable $\tau = \log(Q/Q_{eff})$. The Eq. (2) is valid only for particles with ξ around the peak (ξ_0) of the inclusive particle momentum distribution, in the range $|\Delta\xi| \sim 1$. In theory parameters r_0, r_1, and r_2 are calculated separately for quark and gluon jets [6]. It can be shown that for the ratio of average multiplicities in gluon and quark jets $r = \frac{<n_g>}{<n_q>} = 1.8$ [14], they are:

$$r_0^q = 1.6 - \frac{0.49}{\sqrt{\tau}}, \qquad r_1^q = \frac{1.25}{\tau^{3/2}}, \qquad r_2^q = -\frac{1.8}{\tau^2}, \tag{3}$$

$$r_0^g = 1.33 - \frac{0.28}{\sqrt{\tau}}, \qquad r_1^g = \frac{0.71}{\tau^{3/2}}, \qquad r_2^g = -\frac{1.0}{\tau^2}. \tag{4}$$

The theoretical prediction of the shape of the two-particle momentum correlation distribution function is shown in Fig. 2. The distribution has ridge-like shape. Its central diagonal profiles $\Delta\xi_1 = \Delta\xi_2$ and $\Delta\xi_1 = -\Delta\xi_2$ have linear and parabolic shape, respectively. The general features predicted are that the correlation should be largest for particles with equal momenta $\Delta\xi_1 = \Delta\xi_2$, and the strength of this effect should increase towards larger values of ξ.

B. Local Parton-Hadron Duality

LPHD is a hadronization conjecture that suggests that the properties of hadrons and partons are closely related. In the simplest interpretation of LPHD, each parton at the end of the shower picks up a color matching partner from the vacuum sea and forms a hadron. Within LPHD, one relates particle momentum distributions of hadrons to those of partons via an energy-independent constant K_{LPHD}:

$$\frac{dN_{hadrons}}{d\xi} = K_{LPHD} \cdot \frac{dN_{partons}}{d\xi}. \tag{5}$$

In the two-particle momentum correlation (1), the K_{LPHD} constant cancels out, suggesting that the correlation distributions for partons and hadrons have to be the same. Past studies of inclusive particle distributions at e^+e^- experiments and CDF [3] gave strong support to this hypothesis. In this analysis we further test LPHD by verifying whether the two-particle momentum correlation also survives the hadronization.

C. Normalization

NLLA correlation function from Eq. (1) entangles two effects: multiplicity fluctuations of particles in a jet and actual momentum correlations. In this analysis we wish to measure purely momentum correlations. This can be achieved by introducing one- and two- particle momentum distributions normalized to unity:

$$D'(\xi) = \frac{D(\xi)}{< n >}, \qquad \int D'(\xi) d\xi = 1, \tag{6}$$

$$D'(\xi_1, \xi_2) = \frac{D(\xi_1, \xi_2)}{< n(n-1) >}, \qquad \int\int D'(\xi_1, \xi_2) d\xi_1 d\xi_2 = 1. \tag{7}$$

The correlation function is then:

$$C(\Delta\xi_1, \Delta\xi_2) = \frac{D'(\xi_1, \xi_2)}{D'(\xi_1) D'(\xi_2)} = \frac{< n >^2}{< n(n-1) >} R(\Delta\xi_1, \Delta\xi_2) = \frac{1}{F(\tau)} R(\Delta\xi_1, \Delta\xi_2), \tag{8}$$

where $F(\tau) = \frac{<n(n-1)>}{<n>^2}$ is the second binomial moment. The explicit dependence of binomial moments on energy scale for quark and gluon jets was taken from theory [15]:

$$F_q(\tau) = 1.6 - \frac{1.016}{\sqrt{\tau}}, \qquad F_g(\tau) = 1.33 - \frac{0.58}{\sqrt{\tau}}. \tag{9}$$

D. Quark and Gluon Jets

In NLLA, correlation functions are calculated for quark and gluon jets separately. However, dijet events at the Tevatron consist of both quark and gluon jets. Therefore, in order to compare data to theory, one needs to rewrite the formula for particle momentum distributions as follows:

$$D(\xi) = f_g D_g(\xi) + (1 - f_g) D_q(\xi), \tag{10}$$

$$D(\xi_1, \xi_2) = f_g D_g(\xi_1, \xi_2) + (1 - f_g) D_q(\xi_1, \xi_2), \tag{11}$$

where f_g is a fraction of gluon jets in the sample. It can be shown, that the momentum correlation of Eq. (8) is then:

$$C(\Delta\xi_1, \Delta\xi_2) = c_0 + c_1(\Delta\xi_1 + \Delta\xi_2) + c_2(\Delta\xi_1 - \Delta\xi_2)^2, \tag{12}$$

where c_0, c_1 and c_2 can be expressed in terms of r_0, r_1 and r_2:

$$c_i = \frac{f_g r^2}{f_g r^2 F_g + (1 - f_g) F_q} r_i^g + \frac{1 - f_g}{f_g r^2 F_g + (1 - f_g) F_q} r_i^q, \tag{13}$$

where $r = \frac{<n_g>}{<n_q>}$ and $i = 0, 1, 2$.

III. EVENT SELECTION

A. Triggers

The results presented in this paper are based on data collected from February 2002 to August 2004. Events were accumulated using a single calorimeter tower trigger with E_T threshold of 5 GeV and single jet triggers with E_T thresholds of 20, 50, 70 and 100 GeV, each having different prescales in order not to saturate the available bandwidth.

B. Jet Reconstruction Algorithm

Jets are reconstructed based on the calorimeter information using a cone algorithm [16]. Starting with the highest E_T tower , the algorithm forms preclusters from an unbroken chain of continuous seed towers with transverse energy above 1 GeV provided the towers are within a window of 7x7 towers centered at the originating one. If a seed tower is outside this window, it is used to form a new precluster. The coordinates of the precluster are E_T-weighted sums of ϕ and η of the seed towers within this precluster. In the next step, all towers with $E_T > 0.1$ GeV within $R = \sqrt{(\Delta\phi)^2 + (\Delta\eta)^2} = 1.0$ of the precluster are merged into a cluster. This procedure of calculating coordinates and producing a set of clusters is iterated until a set of clusters is stable. A cluster is stable when the tower list is unchanged from one iteration to the next. The raw transverse energy of a jet is the sum of the transverse energies of the towers belonging to the corresponding cluster. Corrections are applied to the raw energy to compensate for the non-linearity and non-uniformity of the energy response of the calorimeter, the energy deposited inside the jet cone from sources other than the leading parton and the leading parton energy deposited outside the jet cone. A detailed description of this procedure can be found in [17].

C. Offline Selection

Cosmic ray events are rejected by using a cut on the missing transverse energy $\not\!\!E_T$ [18] significance, defined as $\not\!\!E_T/\sqrt{\Sigma E_T}$, where $\Sigma E_T = \Sigma_i E_T^i$ is the total transverse energy of the event, as measured using calorimeter towers with E_T^i above 100 MeV. The cut values are 3.0 GeV$^{1/2}$ for data collected using single tower trigger with E_T threshold of 5 GeV, and 3.5, 5.0, 6.0 and 7.0 GeV$^{1/2}$ for data collected using jet triggers with thresholds of 20, 50, 70 and 100 GeV, respectively. We require that there is one and only one primary vertex in the event, with a z-position $|z| < 60$ cm.

To ensure robust and high efficiency track reconstruction and applicability of the background removal technique (see Sec.V(B)), only events with both leading jets in the central region ($|\eta| < 0.9$) are selected. To reject events with poorly measured jets, we require the two leading jets to be well balanced in E_T: $|k_\perp|/(E_T^1 + E_T^2) < 2\sigma_{k_\perp}$, where E_T^1 and E_T^2 are the transverse energies of the first and the second leading jets, respectively, and:

$$k_\perp = \sqrt{k^2 - k_{||}^2}, \tag{14}$$

$$k_{||} = 2 \cdot cos(\phi/2) \cdot (E_T^1 + E_T^2), \tag{15}$$

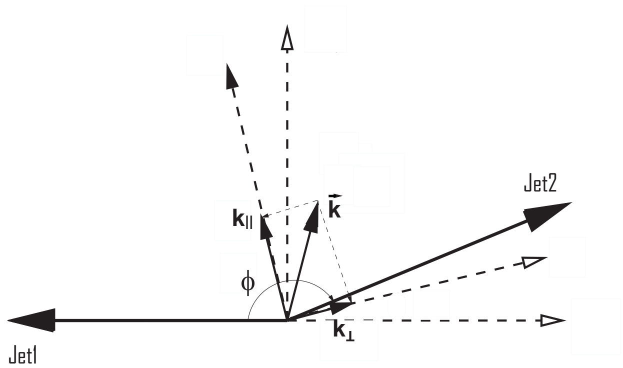

FIG. 3: Illustration of the used jet balance cut. $\vec{k}$ represents a vector sum of transverse momenta of the two leading jets. $\vec{k_{||}}$ and $\vec{k_{\perp}}$ represent the components of $\vec{k}$, parallel and perpendicular to the bisector.

where ϕ is the angle between the two leading jets in the transverse plane, and $\sigma_{k_\perp}$ is the resolution of $k_\perp$. The illustration of $\vec{k}$, $\vec{k_\perp}$ and $\vec{k_{||}}$ is shown in Fig.3. The parameter $k_\perp$ is known to be sensitive to the jet energy mismeasurement, while $k_{||}$ is more sensitive to the hard gluon radiation.

In events with high energy jets, a single track emerging from a jet at a sufficiently large angle with respect to jet axis can be identified as a separate jet. A jet can also be produced from the underlying event. Therefore, rejection of all events with more than two jets can introduce possible biases. We allow up to two extra jets, but their energy is required to be small: $6 < E_T^{extra} < 5.5 + 0.065(E_T^1 + E_T^2)$, where E_T^{extra} is the transverse energy of the extra jet.

After application of selection cuts the final sample consists of approximately 250000 events and is further divided into seven bins according to the dijet mass energy as measured by the calorimeters and defined as:

$$M_{jj} = \sqrt{(E_1 + E_2)^2/c^4 - (\vec{P}_1 + \vec{P}_2)^2/c^2}, \tag{16}$$

where E and $\vec{P}$ are the energies and momenta of jets, respectively. The mass bin boundaries, average invariant mass $< M_{jj} >$ and number of events in each bin are given in Table I.

TABLE I: Dijet mass bins boundaries, average invariant dijet mass $< M_{jj} >$ and number of events in each bin after the event selection cuts.

Bin	Low edge (GeV/c^2)	High edge (GeV/c^2)	Av.Invariant Mass (GeV/c^2)	Number of events
1	66	95	76	15229
2	95	132	108	77246
3	132	180	149	17682
4	180	243	202	80608
5	243	323	272	18528
6	323	428	361	12000
7	428	563	475	19150

IV. TRACK SELECTION, CORRECTIONS

All measurements are performed in the dijet center of mass frame. The correlation distributions are measured for all tracks passing track quality cuts and within the restricted cones of opening angle $\theta_c = 0.5$ radians relative to the jet axis. Backgrounds, both correlated and uncorrelated with jet direction, are considered and corrected for.

A. Track Quality Cuts

Several cuts are applied to ensure that tracks in the measurement do originate from the primary vertex and are not produced by cosmic rays, multiple interactions or γ-conversions, K^0 and Λ-decays and other types of backgrounds.

In our analysis, we require the full 3D track reconstruction. The description of CDF track reconstruction can be found in [19][20]. Poorly reconstructed and spurious tracks are removed by requiring $\chi^2_{COT} < 6.0$. Tracks are required to have $p_T > 0.3$ GeV/c.

The parameter Δz, defined as the difference between the z position of the track at the point of its closest approach to the beamline and the z position of the primary vertex, is used to remove tracks not originating from the primary interaction. We require $|\Delta z| < 5 \cdot \sigma_{\Delta z}$. The $\sigma_{\Delta z}$ is determined individually for each category of tracks, based on the number of SVX and COT hits.

Tracks produced in γ-conversions are removed by using a combination of cuts on impact

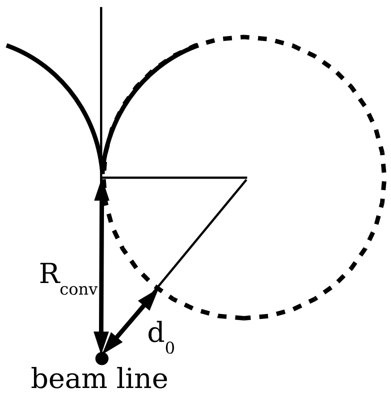

FIG. 4: Illustration of distance R_{conv} from the beam line to the point where the conversion occured.

parameter d_0 and the distance R_{conv} (Fig. 4) from the beam line to the point where the conversion occured. Impact parameter d_0 is defined as the shortest distance in the $r - \phi$ plane between the interaction point and the particle trajectory obtained by the tracking algorithm fit. It can be shown that for electrons and positrons originating from γ-conversion:

$$R_{conv} = \sqrt{\frac{d_0 p_T}{0.15B}} \tag{17}$$

where p_T is the transverse momentum of the charged particle in GeV/c, B is the magnetic field in Tesla and R_{conv} is measured in meters. The sign of R_{conv} is selected to be positive if $d_0 \cdot q > 0$, and negative if $d_0 \cdot q < 0$, where q is the charge of the particle. Monte Carlo studies indicated that d_0 cut alone is less efficient in removing γ-conversion tracks than a combination cut. Tracks used in the measurement are required to have $|d_0| < 5 \cdot \sigma_{d_0}$ or $R_{conv} < 13$ cm. The value $R_{conv} = 13\ cm$ was motivated by the location of SVX portcards. The resolution of the impact parameter σ_{d_0} is evaluated separately for each category of tracks, based on the number of SVX and COT hits.

To verify the efficiency of applied track quality cuts, we compare distributions of inclusive mean multiplicity Fig. 5 and inclusive momentum distributions Fig. 6 in a Pythia Tune A sample at generator and reconstructed track levels. This was motivated by the fact that there are no secondary decay particles in the generator level distributions. The agreement after selection cuts confirms that selected cuts do remove most of the background tracks. The effect of the remaining fraction of secondary tracks is estimated by comparing correlation distributions $C(\Delta\xi_1, \Delta\xi_2)$ at charged hadron and reconstructed track levels in Monte Carlo and a corresponding bin-by-bin scale factor is produced. The difference between

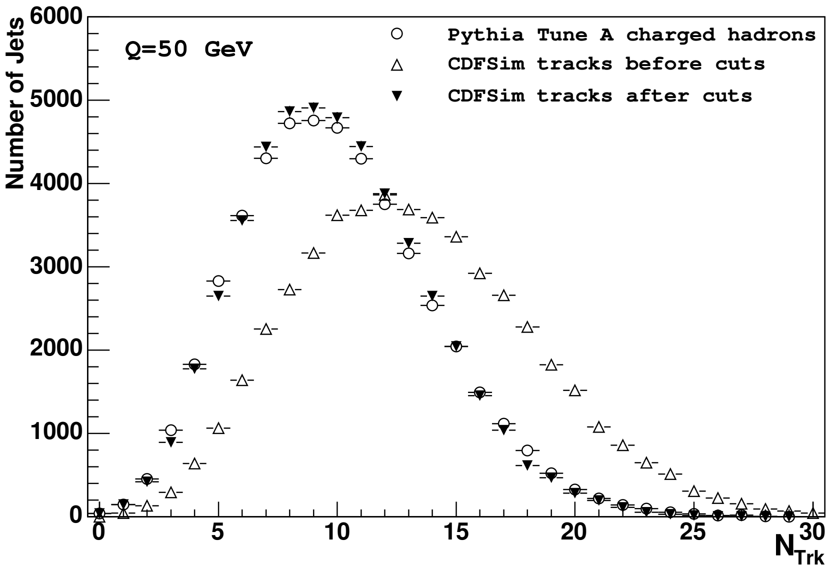

FIG. 5: Average particle multiplicity in the jet for $Q = 50$ GeV before and after cuts.

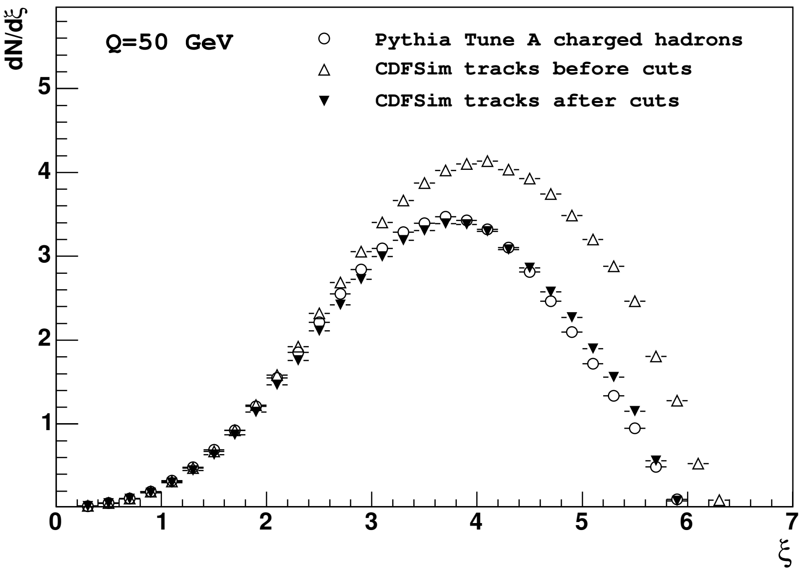

FIG. 6: Inclusive momentum distribution of particles in the jet for $Q = 50$ GeV before and after cuts.

distributions in data, with and without this scale factor applied, is assigned as the systematic uncertainty due to the track quality cuts.

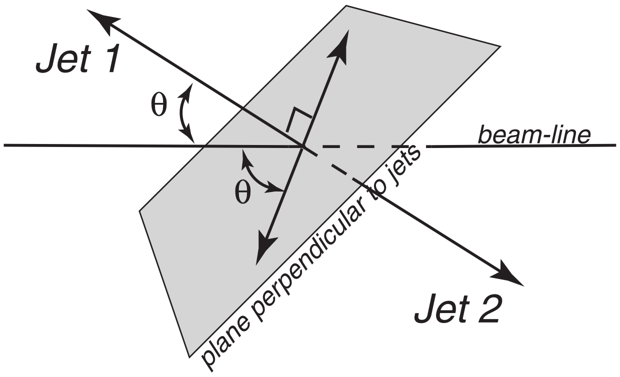

FIG. 7: Illustration of the complementary cones.

B. Uncorrelated Background Subtraction

In order to remove contributions due to the underlying event, accelerator induced backgrounds and particles from not reconstructed secondary interactions in the same bunch-crossing, additional corrections still need to be applied. We use the complementary cone technique to estimate this effect. Two complementary cones are positioned at the same polar angle with respect to the beam-line as the original jets and rotated in ϕ so that they are at 90^o (i.e. as far as possible) with respect to the dijet axis, as shown in Fig. 7. Geometrically this can be done only when the dijet axis is within $45^o < \theta < 135^o$. We assume that cones formed in such a fashion collect statistically the same amount of uncorrelated background as the cones around the jet axis [5].

In order to obtain the corrected expression for $C(\Delta\xi_1, \Delta\xi_2)$, one needs to subtract the background from the one- and two-particle momentum distributions. This can be achieved by considering particles in jet and complementary cones together. It can be shown that the momentum distributions with the background subtracted are:

$$D(\xi) = D(\xi^{jet}) - D(\xi^{compl}) \tag{18}$$

$$D(\xi_1, \xi_2) = 2D(\xi_1^{jet}, \xi_2^{jet}) - D(\xi_1^{jet+compl.}, \xi_2^{jet+compl.}) + 2D(\xi_1^{compl.}, \xi_2^{compl.}) \tag{19}$$

where $jet+compl$ indicates that a particle can be in either jet cone or complementary cone.

C. Effect of Tracking Inefficiency

High efficiency of track reconstruction is ensured by selecting events with central jets and eliminating poorly reconstructed and spurious tracks. However, there still may be some non-reconstructed tracks inside the jet. To evaluate the corresponding systematic uncertainty, we have modeled track reconstruction efficiency using the function $P(\xi) = p_1 + p_2\xi$, indicating the probability of reconstructing a track with given ξ. Values of parameters p_1 and p_2 were varied. The CDF tracking efficiency has increased since Run I and is known to be higher than one estimated using our function. Correlation distributions show very weak dependence on tracking inefficiency, even within the context of this model which underestimates actual tracking efficiency.

D. Neutral Particles

Theoretical predictions of correlation distributions are done at parton level, while LPHD allows one to connect final partons to hadrons, assuming that all hadrons are counted. The analysis, however, is done for charged particles only. To estimate this effect, the momentum correlation in Pythia Tune A sample is compared for charged only and all particles. The difference is assigned as the corresponding systematic uncertainty.

E. Resonance Decays

The presence of resonance decays might be expected to cause an offset between data and theory. We examine this effect by comparing correlations in Monte Carlo at the level of final hadrons and before resonance decays. We found that this results in insignificant changes of $C(\Delta\xi_1, \Delta\xi_2)$ and does not change the overall level of correlation.

V. NLLA FITS TO DATA

The two-particle momentum correlation distributions $C(\Delta\xi_1, \Delta\xi_2)$ are produced for seven bins of dijet mass.

The distributions have ridge-like shape as predicted by theory. In this paper we report the central diagonal profiles $\Delta\xi_1 = -\Delta\xi_2$ and $\Delta\xi_1 = \Delta\xi_2$ (shown on Fig. 2) of the distributions.

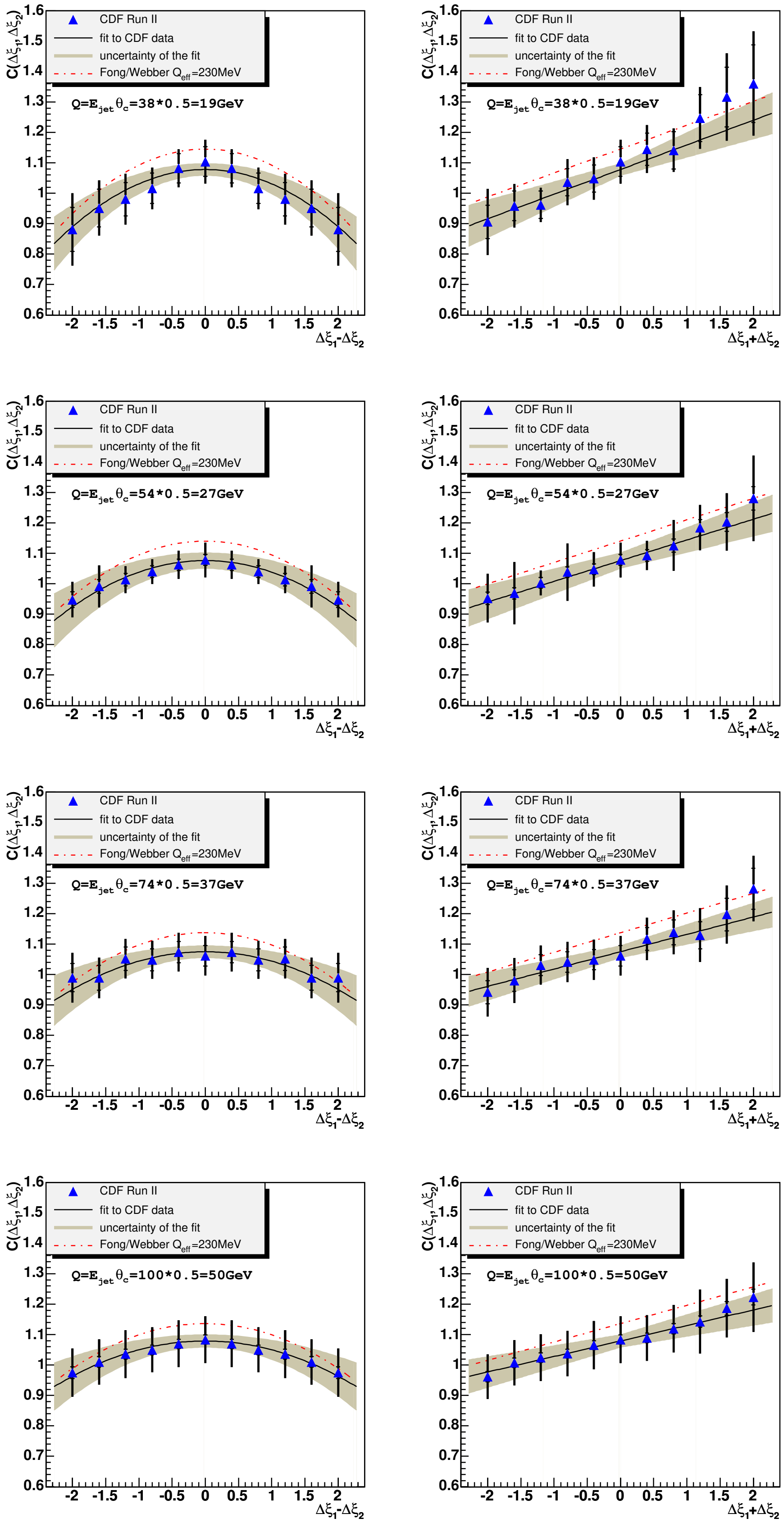

CDF Run II
fit to CDF data
uncertainty of the fit
Fong/Webber Q_eff=230MeV
Q=E_jet θ_c=38*0.5=19GeV
Q=E_jet θ_c=54*0.5=27GeV
Q=E_jet θ_c=74*0.5=37GeV
Q=E_jet θ_c=100*0.5=50GeV
C(Δξ_1,Δξ_2)
Δξ_1-Δξ_2
Δξ_1+Δξ_2

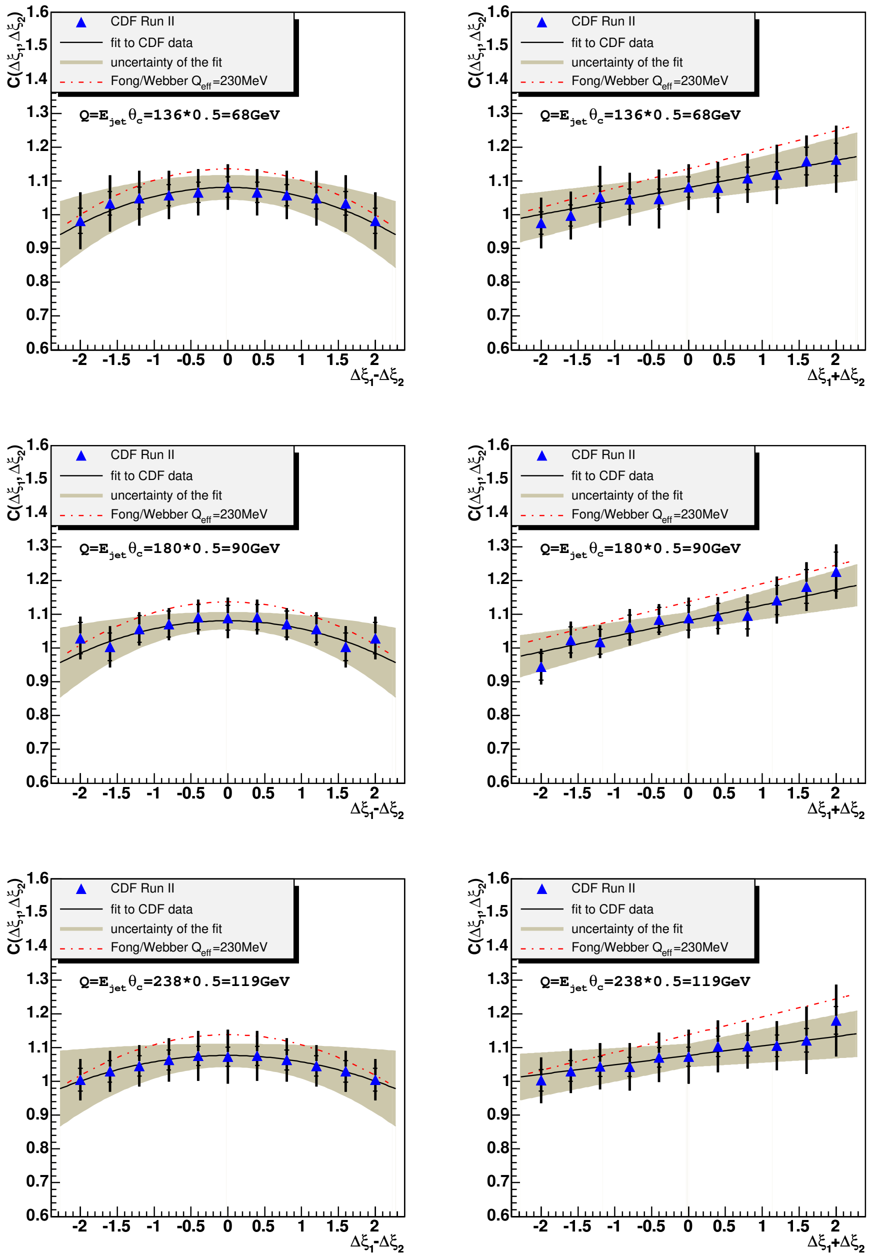

FIG. 8: Comparison of momentum correlation in data and theory. Central diagonal profiles $\xi_1 = -\xi_2$ and $\xi_1 = \xi_2$ are shown.

Fig. 8 shows diagonal profiles corresponding to the seven available dijet mass bins. The bin size $\Delta\xi = 0.2$ is chosen to be much wider than the momentum resolution in the fitted range. Smaller error bars correspond to statistical uncertainty only, while larger ones to statistical and systematic uncertainties added in quadrature. The solid line corresponds to the NLLA fits according to Eq.(12) with three free parameters c_0, c_1 and c_2. The fit range ± 2 in

TABLE II: Summary of the fitted correlation parameters.

Q (GeV)	c_0	c_1	c_2
19	$1.078 \pm 0.007 \pm 0.016$	$0.081 \pm 0.006 \pm 0.016$	$-0.047 \pm 0.006 \pm 0.008$
27	$1.076 \pm 0.003 \pm 0.022$	$0.068 \pm 0.002 \pm 0.015$	$-0.038 \pm 0.002 \pm 0.012$
37	$1.075 \pm 0.005 \pm 0.018$	$0.057 \pm 0.004 \pm 0.013$	$-0.031 \pm 0.004 \pm 0.012$
50	$1.079 \pm 0.002 \pm 0.019$	$0.051 \pm 0.002 \pm 0.014$	$-0.029 \pm 0.002 \pm 0.010$
68	$1.081 \pm 0.004 \pm 0.028$	$0.040 \pm 0.004 \pm 0.012$	$-0.027 \pm 0.004 \pm 0.011$
90	$1.081 \pm 0.005 \pm 0.023$	$0.046 \pm 0.004 \pm 0.015$	$-0.024 \pm 0.004 \pm 0.014$
119	$1.077 \pm 0.004 \pm 0.033$	$0.028 \pm 0.003 \pm 0.015$	$-0.019 \pm 0.003 \pm 0.015$

$\Delta\xi_1 + \Delta\xi_2$ and $\Delta\xi_1 - \Delta\xi_2$ was motivated by the region of validity of NLLA calculations. On one hand, NLLA imposes a limitation on the allowed transverse momentum k_T of the particles with respect to the jet ($k_T > Q_{eff}$), on another it requires particles to have low momentum, so that $p/E_{jet} \ll 1$. The extracted values of the fit parameters are reported in Table II. Dashed line corresponds to the theoretical curve given by Eq. (12) for the value of $Q_{eff} = 230$ MeV, extracted from fits of inclusive momentum distributions in CDF Run I [5]. The fraction of gluon jets in the sample, needed to calculate the theoretical prediction for a mixture of quark and gluon jets, is obtained from Pythia Tune A with CTEQ5L parton distribution functions [21].

The overall qualitative agreement between data and NLLA calculations is very good. Data follows theoretical trends, indicating an enhanced probability of finding two particles with the same value of momenta (parabolic shape of $\Delta\xi_1 = -\Delta\xi_2$ diagonal profile with its maximum at 0) and that this effect is becoming larger for particles with lower momenta (positive slope of $\Delta\xi_1 = \Delta\xi_2$ diagonal profile). A small offset in the overall level of correlation is observed in all seven dijet mass bins, indicating that theory overestimates parameter c_0 of the correlation.

Fig.9 shows evolution of parameters c_0, c_1, and c_2 with jet hardness Q. Each data point corresponds to the value of the parameter measured in a particular dijet mass bin. Distributions are fit to NLLA function with Q_{eff} treated as the only free parameter, fits are represented by solid lines. Theoretical curves for pure quark and gluon jets in the final state are also shown. The value of Q_{eff} is extracted from each of these three fits individually.

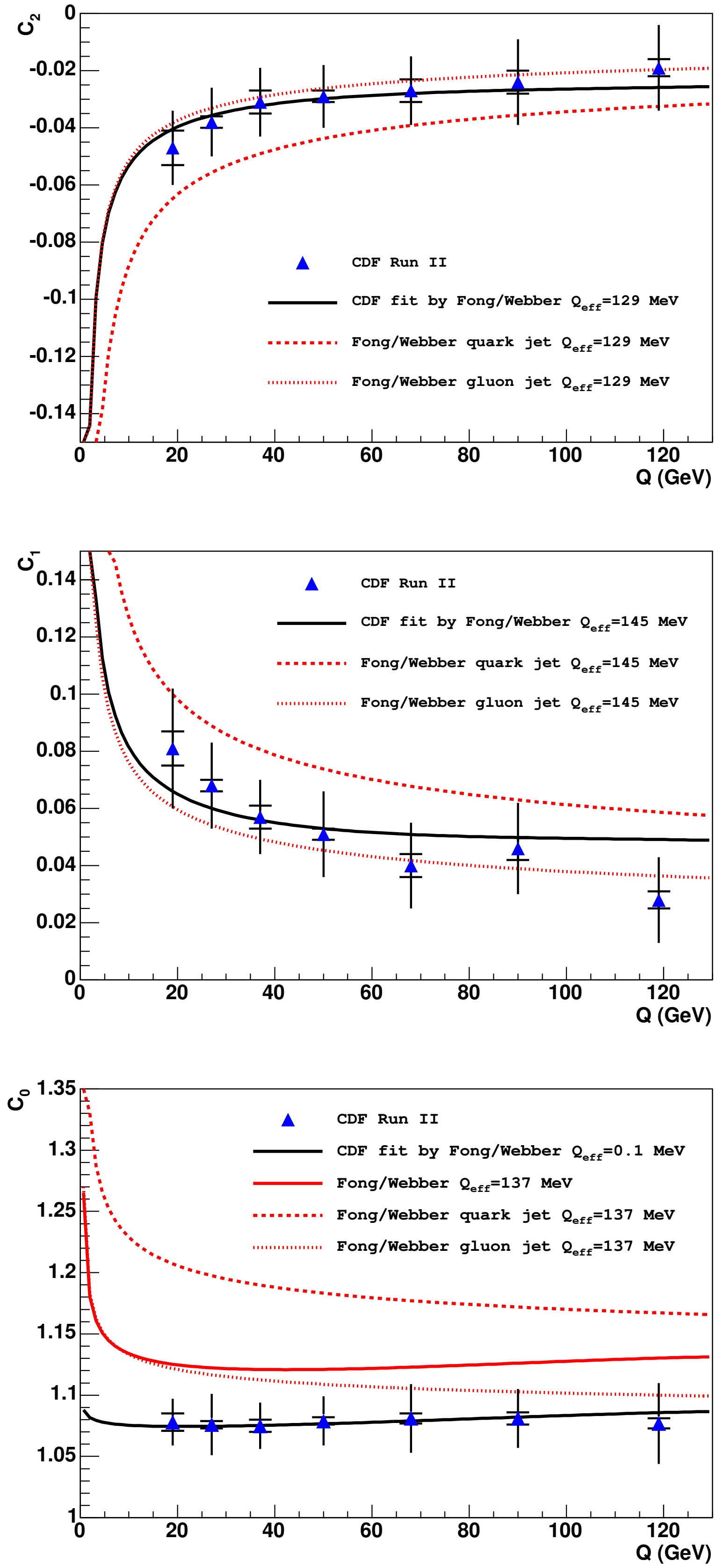

FIG. 9: Evolution of correlation parameters with energy.

Systematic uncertainties for these values are estimated by varying the respective corrections and cuts and refitting the distributions for the parameter Q_{eff}. Systematic uncertainty due to choice of parton distribution function set is evaluated by comparing results for the fraction of gluon jets f_g obtained using CTEQ5L and CTEQ6.1 ([22]) PDF sets. The systematic error due to the uncertainty of the value of r was evaluated by taking a difference between theoretical $r = 9/4$ and experimentally measured $r = 1.8$ [14] values and propagating it to the value of Q_{eff}. Both uncertainties appear to be small compared to other sources and, propogated to the value of Q_{eff}, never exceeded 3%.

The evolution of correlation parameters with energy show the same trends in data and theory. The value of Q_{eff} obtained from the fit of c_1 is $147 \pm 10(stat) \pm 79(syst) \pm 2(pdf)$ MeV. The value of Q_{eff} obtained from the fit of c_2 is $131 \pm 12(stat) \pm 86(syst) \pm 3(pdf)$ MeV. Evolution of c_0 has an offset of ~ 0.06. Note that c_0 is sensitive to the definition of the expansion point ξ_0. A formal fit to theoretical function gives the value of $Q_{eff} = 0.1$ MeV. This value, however, does not have physical meaning as the distributions of c_0 vs Q in data and theory are not in agreement. Other than the offset, c_0 shows very weak Q dependence, as expected from theory.

VI. COMPARISON TO MONTE-CARLO

We compare momentum correlation distributions of charged particles in data to Pythia Tune A and Herwig 6.5 predictions. Predictions of Monte-Carlo generators are in agreement with each other and with results obtained in data. Fig.10 shows the central diagonal profiles of correlation distributions in data compared to Pythia Tune A and Herwig 6.5 predictions at the level of final charged hadrons.

VII. SUMMARY

In this analysis we measured two-particle momentum correlation distributions of charged particles in jets from dijet events in a wide range of dijet masses 70-560 GeV/c^2. The jets were produced in $p\bar{p}$ collisions at center of mass energy of 1.96 TeV. The measurement was made for particles in a restricted cone around the jet direction with opening angle $\theta_c = 0.5$ radians.

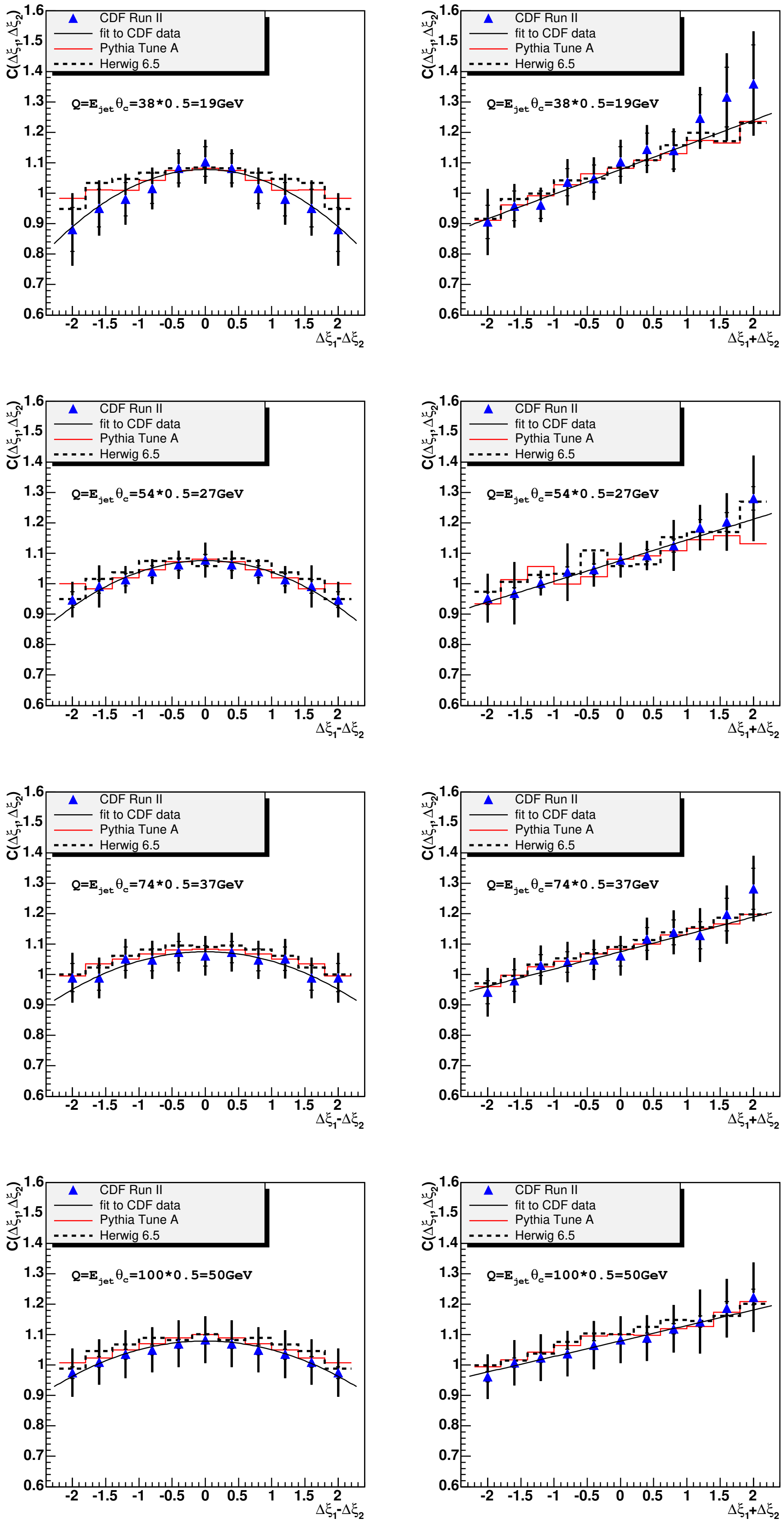
CDF Run II
fit to CDF data
Pythia Tune A
Herwig 6.5
C(Δξ1,Δξ2)
Q=E_jet θ_c=38*0.5=19GeV
Q=E_jet θ_c=54*0.5=27GeV
Q=E_jet θ_c=74*0.5=37GeV
Q=E_jet θ_c=100*0.5=50GeV
Δξ1-Δξ2
Δξ1+Δξ2

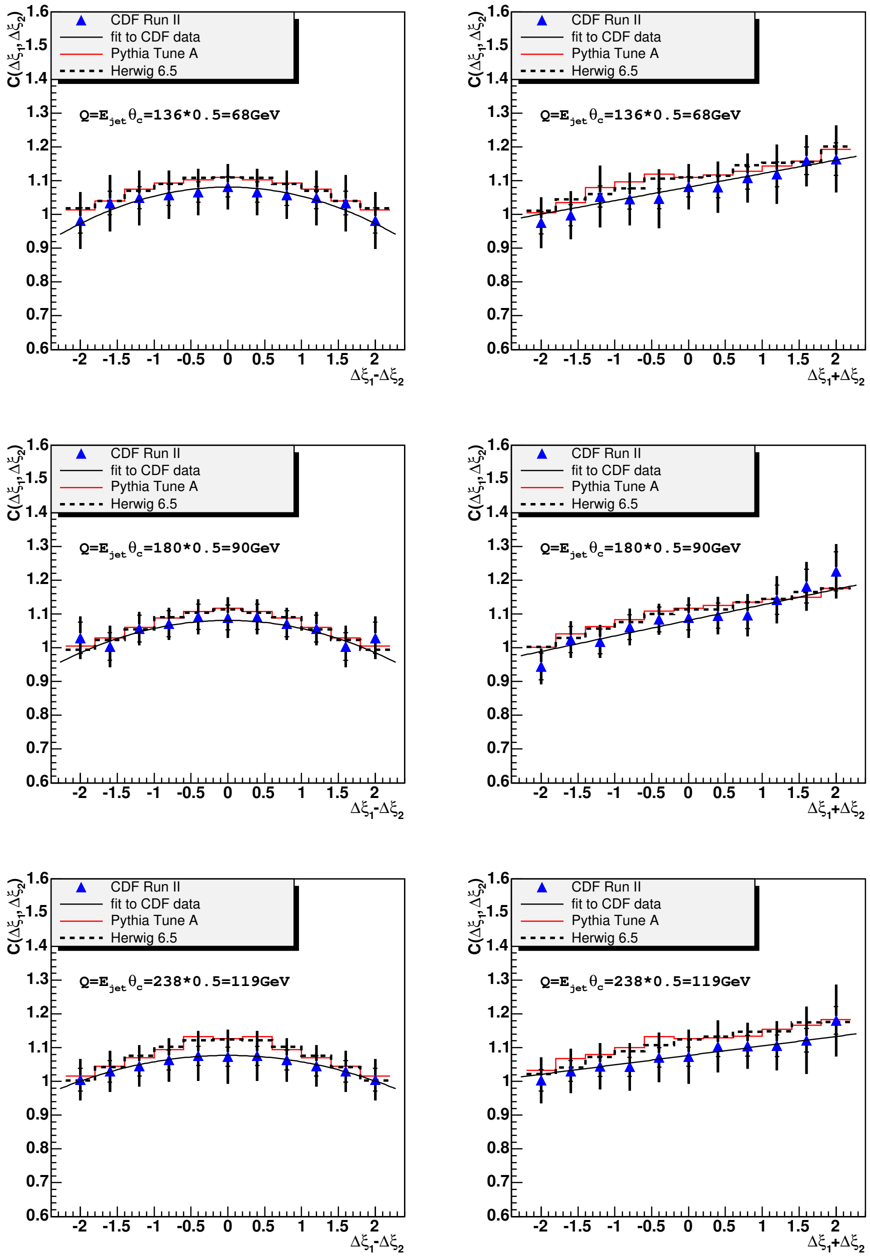

FIG. 10: Comparison of momentum correlation in data to Pythia Tune A and Herwig 6.5 Monte-Carlo event generators at charged hadron level. Central diagonal profiles $\xi_1 = -\xi_2$ and $\xi_1 = \xi_2$ are shown.

The data were compared to the Next-to-Leading-Log Approximation calculations combined with the hypothesis of Local Parton-Hadron Duality. Overall, data and theory showed the same trends in the entire range of dijet masses. The parton shower cut-off scale Q_{eff} was extracted from fits of the evolution of correlation parameters. The average value of Q_{eff} extracted from the fits of c_1 and c_2 appears to be reasonable: $139 \pm 11(stat) \pm 84(syst) \pm 3(pdf)$ MeV. Even though the evolution of c_0 shows the same behaviour as in theory, the fit of c_0 vs Q gives an unreasonably low value of $Q_{eff} = 0.1$ MeV due to a constant offset observed at all energies. Both Monte-Carlo event generators, Pythia Tune A and Herwig 6.5, were found to reproduce the correlations in data fairly well. The results of this analysis indicate that the parton momentum correlation survive the hadronization stage of jet fragmentation, giving further support to the hypothesis of LPHD.

VIII. ACKNOWLEGDEMENTS

We thank the Fermilab staff and the technical staffs of the participating institutions for their vital contributions. This work was supported by the U.S. Department of Energy and National Science Foundation; the Italian Istituto Nazionale di Fisica Nucleare; the Ministry of Education, Culture, Sports, Science and Technology of Japan; the Natural Sciences and Engineering Research Council of Canada; the National Science Council of the Republic of China; the Swiss National Science Foundation; the A.P. Sloan Foundation; the Bundesministerium fuer Bildung und Forschung, Germany; the Korean Science and Engineering Foundation and the Korean Research Foundation; the Particle Physics and Astronomy Research Council and the Royal Society, UK; the Russian Foundation for Basic Research; the Comision Interministerial de Ciencia y Tecnologia, Spain; and in part by the European Community's Human Potential Programme under contract HPRN-CT-2002-00292, Probe for New Physics.

---

[1] Yu. Dokshitzer, V. Khoze, A. Mueller, and S. Troyan, *Basics of Perturbative QCD*, edited by J. Tran Thanh Van (Editions Frontières, Gif-sur-Yvette, 1991).

[2] Ya.I. Azimov, Yu. Dokshitzer, V. Khoze, and S. Troyan, Z. Phys. C **27**, 65 (1985);ibid. **31**, 213 (1986).

[3] G. Alexander *et al.* (OPAL Collaboration), Phys. Lett. B **265**, 462 (1991); P.D. Acton *et al.* (OPAL Collaboration), Z. Phys. C **58**, 387 (1993); R. Akers *et al.* (OPAL Collaboration), Z. Phys. C **68**, 179 (1995); D. Busculic *et al.* (ALEPH Collaboration), Phys. Lett. B **346**, 389 (1995); G. Alexander *et al.* (OPAL Collaboration), Phys. Lett. B **388**, 659 (1996);

D. Busculic *et al.* (ALEPH Collaboration), Phys. Lett. B **384**, 353 (1996); P. Abreu *et al.* (DELPHI Collaboration), Z. Phys. C **70**, 179 (1996); K. Ackerstaff *et al.* (OPAL Collaboration), Eur. Phys. J. C **1**, 479 (1998); P. Abreu *et al.* (DELPHI Collaboration), Phys. Lett. B **449**, 383 (1999); K. Abbiendi *et al.* (OPAL Collaboration), Eur. Phys. J. C **11**, 217 (1999); Y. Iwasaki, for SLD Collaboration, SLAC-R-95-460, SLAC preprint, Stanford, 1995.

[4] T. Affolder *et al.* (CDF Collaboration), Phys. Rev. Lett. **87**, 211804 (2001).

[5] D. Acosta *et al.* (CDF Collaboration), Phys. Rev. D **68**, 012003 (2003).

[6] C. Fong and B.R. Webber, Phys. Lett. B **229**, 289 (1989); C. Fong and B.R. Webber, Phys. Lett. B **241**, 255 (1989); C. Fong and B.R. Webber, Nucl. Phys. B **355**, 54 (1991).

[7] R. Perez Ramos, JHEP **0606**, 019 (2006).

[8] G. Acton *et al.* (OPAL Collaboration), Phys. Lett. B **287**, 401-412 (1992).

[9] M.Z. Akrawy *et al.* (OPAL Collaboration), Phys. Lett. B **247**, 617 (1990).

[10] T. Sjostrand, Phys. Lett. B **157** , 321 (1985); M. Bengtsson, T. Sjostrand, and M. van Zijl, Z. Phys. C **32**, 67, (1986); T. Sjostrand and M. van Zijl, Phys. Rev. D **36**, 2019 (1987).

[11] R. Field, presented at Fermilab ME/MC Tuning Workshop, Fermilab, October 4, 2002; R. Field and R.C. Group [CDF Collaboration], arXiv:hep-ph/0510198.

[12] G. Marchesini and B.R. Webber, Nucl. Phys. B **310**, 461 (1988); I. G. Knowles, Nucl. Phys. B **310**, 571 (1988); S. Catani, G. Marchesini, and B.R. Webber, Nucl. Phys. B **349**, 635 (1991).

[13] A.H. Mueller, in Proc.1981 Int. Symp. on Lepton and Photon Interactions and Energies, ed. W. Pfeil (Bonn, 1981), p.689; Yu.L. Dokshitzer, V.S. Fadin and V. Khoze, Phys. Lett. B **115**, 242 (1982); A.H. Mueller, Nucl. Phys. B **213**, 85 (1983); ibid. B **241**, 141 (1984).

[14] D. Acosta *et al.* (CDF Collaboration), Phys. Rev. Lett. **94**, 171802 (2005); A. Pronko, Int. J. Mod. Phys., A **20**, 3723 (2005); A. Pronko, Acta Phys. Polon., B **36**, 451 (2005).

[15] Yu.L. Dokshitzer, V.A. Khoze and S.I. Troyan, in Perturbative Quantum Chromodinamics, ed. A.H. Mueller (World Scientific, Singapore, 1989), p. 241; E.D. Malaza and B.R. Webber, Phys. Lett. B **149**, 501 (1984); E.D. Malaza and B.R. Webber, Phys. Lett. B **267**, 702 (1986); K. Tesima, Phys. Lett. B **221**, 91 (1989).

[16] F. Abe *et al.*, Phys. Rev. D **45**, 1448 (1992).

[17] A. Bhatti *et al.*, Nucl. Instrum. Meth. A **566**, 375 (2006) [arXiv:hep-ex/0510047].

[18] $\not{E}_T$ is defined as the norm of -$\Sigma_i E_T^i \cdot \vec{n_i}$, where $\vec{n_i}$ is the unit vector in the azimuthal plane that points from the beamline to the i-th calorimeter tower.

[19] The CDF II Detector Technical Design Report, Fermilab-Pub-96/390-E.

[20] C. Hays *et al.*, Nucl. Instrum. Meth. A **538**, 249 (2005).

[21] J. Pumplin, *et al.*, Eur. Phys. J. C **12**, 375 (2000).

[22] D. Stump *et al.*, JHEP **0310**, 046 (2003).